GFRP Reinforced Bridge Barriers: Impact Experiment

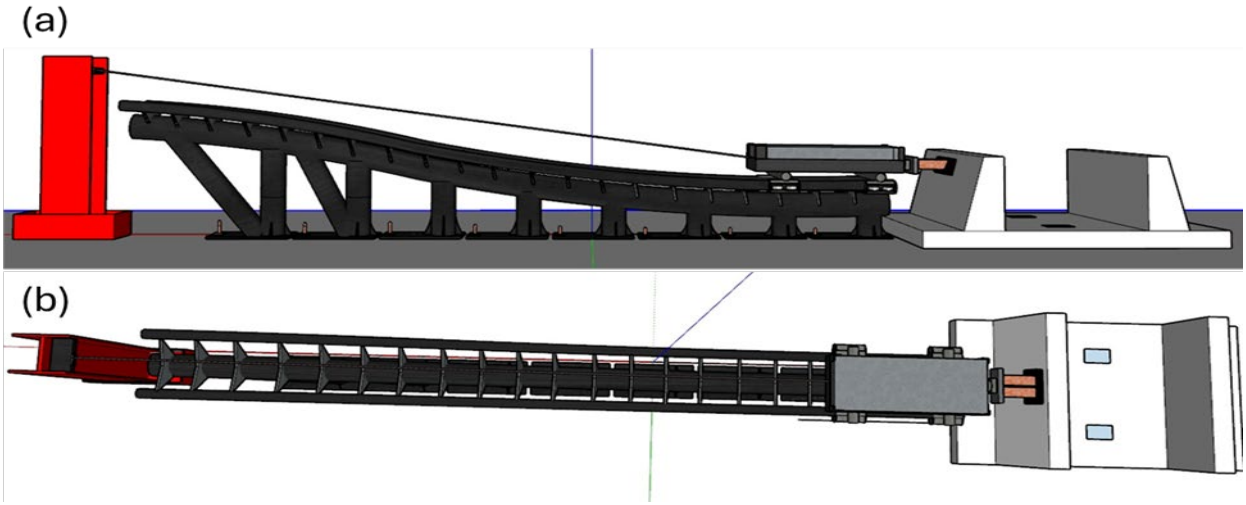

June 2025
Final Report

Project number TR202319
MoDOT Research Report number 25-010

PREPARED BY:

Congjie Wei, Ph.D.

Manish Kumar Gadhe

John J. Myers, Ph.D.

Chenglin Wu, Ph.D.

Missouri University of Science and Technology

PREPARED FOR:

Missouri Department of Transportation

Construction and Materials Division, Research Section

TECHNICAL REPORT DOCUMENTATION PAGE

1. Report No. cmr 25-010	**2. Government Accession No.**	**3. Recipient's Catalog No.**
4. Title and Subtitle GFRP Reinforced Bridge Barriers: Experiment Testing		**5. Report Date** June 2025 Published: July 2025 **6. Performing Organization Code**
7. Author(s) Congjie Wei, Ph.D. Manish Kumar Gadhe John J. Myers, Ph.D. Chenglin Wu, Ph.D.		**8. Performing Organization Report No.**
9. Performing Organization Name and Address Department of Civil, Architectural and Environmental Engineering Missouri University of Science and Technology 1401 N. Pine St. Rolla, MO 65409		**10. Work Unit No.** **11. Contract or Grant No.** MoDOT project # TR202319
12. Sponsoring Agency Name and Address Missouri Department of Transportation (SPR-B) Construction and Materials Division P.O. Box 270 Jefferson City, MO 65102		**13. Type of Report and Period Covered** Final Report (January 2023-June 2025) **14. Sponsoring Agency Code**

15. Supplementary Notes
Conducted in cooperation with the U.S. Department of Transportation, Federal Highway Administration. MoDOT research reports are available in the Innovation Library at https://www.modot.org/research-publications.

16. Abstract
The reported work includes the experiment testing of glass fiber reinforced polymer (GFRP) and steel reinforced concrete bridge barriers. A total of four reinforced concrete barriers were prepared, including three GFRP reinforced barriers and one mild steel reinforced barrier, and cast on two concrete slabs. Impact testing was conducted using a cart with weight and a long straight sled system. The force, displacement, and strain data were measured. The results demonstrated that GFRP is fully capable of withstanding impact loads that could occur in real-world scenarios.

17. Key Words GFRP reinforced bridge barriers, Impact test, Deformation analysis	**18. Distribution Statement** No restrictions. This document is available through the National Technical Information Service, Springfield, VA 22161.

19. Security Classif. (of this report) Unclassified.	**20. Security Classif. (of this page)** Unclassified.	**21. No. of Pages** 29	**22. Price**

Form DOT F 1700.7 (8-72) Reproduction of completed page authorized

GFRP Reinforced Bridge Barriers: Experimental Testing

Project Number: TR202319

Final Report

Investigator:

Congjie Wei, Post-doctoral Researcher, Texas A&M University

Manish Kumar Gadhe, Master's Student, Missouri S&T

Dr. John J. Myers, Professor, Missouri S&T

Dr. Chenglin Wu, Associate Professor, Texas A&M University

June 2025

COPYRIGHT

DISCLAIMER

ACKNOWLEDGMENTS

The authors would like to acknowledge the many individuals and organizations that made this research project possible. First and foremost, the author would like to acknowledge the financial support of the Missouri Department of Transportation (MoDOT) and the Missouri Center for Transportation Innovation (MCTI). The authors would like to give special thanks to Dr. Bryan Hartnagel, Darren Kemna, Tyler Lindsay, Brent T. Schulte, and Jennifer Harper at MoDOT for their insightful suggestions, comments, and report edits during the research process.

TABLE OF CONTENTS

LIST OF FIGURES

LIST OF TABLES

EXECUTIVE SUMMARY

The primary objective of this research is to design and conduct a series of impact tests on concrete barriers reinforced with glass fiber-reinforced polymer (GFRP), as well as a control test specimen with mild steel reinforcing materials. The GFRP reinforcement consists of a hook-shaped piece and a spiral piece, which form the required confinement to develop the strains of the transverse bars and provide shear resistance. The spiral piece was embedded into the slab to achieve the bending effects needed for the barrier impact. The theoretical feasibility of this design has been demonstrated in our previous project and is detailed in the report titled "GFRP Reinforced Bridge Barriers: Numerical Modeling".

In this work, four concrete barriers were constructed on two concrete slabs. For comparison consideration, three barrier specimens were reinforced with GFRP materials, while one was reinforced with steel. The impact tests were conducted by utilizing an impact cart mounted on a straight, long sled system. Strain gauges, string-pots, load cells, and accelerometers were installed and used to measure force and deformation during and after the impact loading was applied.

The results showed that for all cases, the fluctuations of strain, force, and acceleration quickly returned to zero after a significantly small amount of time. The sustained impact load exceeds the design load. After impact tests, the specimens exhibited no damage or cracks. No significant lateral displacements were observed for the barrier. The strain measured along the GFRP bars shows lower values than the yield strain of the steel, indicating an elastic response of the specimens. These results demonstrate the capability of GFRP-reinforced concrete barriers to withstand the same level of impact force as traditional steel-reinforced concrete barriers.

Keywords: GFRP reinforced bridge barriers, impact test, deformation analysis

1. INTRODUCTION

1.1 Problem Statement

Concrete road barriers are crucial for safeguarding lives on roadways. As a final safety measure, these barriers must effectively prevent vehicles that have lost control from crossing into opposite lanes of traffic or crashing into adjacent fields, scenarios that could result in more severe accidents than collisions with the barriers themselves. Understanding how these barriers behave and potentially fail under various impact conditions, determined from vehicle types, impact angles, and other influential factors, is essential for ensuring their effectiveness [1-5].

Currently, steel is the most commonly used reinforcement material for concrete structures. However, corrosion is a main issue, especially for structures impacted by freezing and thawing environments [6-10] in the Midwest regions. Each year in the US, hundreds of millions of dollars are spent on corrosion-related repair or maintenance projects. If not repaired or maintained effectively, structures impacted by corrosion, such as bridges, could experience a catastrophic failure, which could lead to loss of human life. The corrosion process is triggered by the infusion of chloride and oxygen ions, which is enhanced by the porous solid nature of concrete materials. The electrode reactions at the interface between the reinforcement and concrete materials consume iron and produce ferric oxide, which is also known as rust. These ferric oxides are more than twice the volume of steel and would introduce volumetric compressive strains in the surrounding structure, leading to damage. This causes safety problems by degrading both the reinforcement material's strength and the bond strength between the reinforcements and the concrete.

By replacing steel reinforcement with corrosion-resistant or corrosion-free materials, has been actively pursued in the past decades. For instance, corrosion-free, glass fiber reinforced polymer (GFRP), emerges as a promising alternative to steel reinforcement [11-13]. GFRP does not undergo the corrosive processes that can significantly degrade steel reinforcement, thereby preserving both the structural integrity and the longevity of concrete infrastructure. Utilizing GFRP could lead to safer, more durable construction that withstands harsh environments without the ongoing need for costly repairs and maintenance. This switch not only has the potential to enhance the safety and durability of new structures but also contributes to more sustainable construction practices by reducing the frequency and severity of maintenance interventions. As the construction industry seeks to adapt to the changing needs of modern infrastructure, materials like GFRP offer a viable solution to one of its most pressing challenges [14-17]. However, unlike steel, GFRP has a brittle failure nature, which raises concerns about the potential lack of ductility in GFRP-reinforced concrete structures. Therefore, experimental investigations of GFRP reinforced concrete structures are crucial to reveal the failure modes and design loads in comparison with their steel counterparts.

This project aims to provide experimental evidence on the capability of GFRP-reinforced concrete bridge barriers to withstand impact loading conditions without generating obvious damage or cracking, and to undergo no serviceability loss. A considerable amount of work has already occurred on the experimental testing of different types of steel reinforced concrete barriers [18]. In 2001, the National Transportation Library conducted crash tests on the Oregon Standard (32-in.) F-shape precast concrete barrier and the Oregon Tall (42-in.) F-shape precast

concrete barrier [19]. In 2003, Consolazio et al. reported a series of finite element models and on-site crash tests on low-profile concrete work zone barriers [20]. The California Department of Transportation has also conducted a systematic study on the crush testing of a variety of steel reinforced concrete barriers [21]. However, the application of GFRP materials in concrete bridge barriers following the state-DOT approved designs has been rare, and there are scarce numerical and experimental studies on their performance under impact loading.

1.2. Research Objectives

This project aims to conduct a series of impact tests on GFRP reinforced concrete barriers. For comparison, a traditional steel reinforced concrete barrier with the same size and material setup was also tested.

To fulfil the objectives mentioned, the tasks of this project are summarized as follows:

Task 1: Construct GFRP and Steel-Reinforced Concrete Bridge Barrier Specimens
The first task involved the preparation of specimen barriers for testing. Four reinforced concrete barrier specimens were created, three reinforced with GFRP and one with traditional steel. These barriers were cast face-to-face on two separate concrete slabs to optimize both cost and resource use. Strain, force, and acceleration measurement systems were installed within and on the concrete barriers to record the deformation and behavior under the impact load.

Task 2: Conduct Impact Testing
A specialized crash test sled system, previously developed by the pool-fund study led by Prof. Mohammed ElGawady, was employed to deliver controlled impacts to the barriers, mimicking actual vehicular collision scenarios. This test was designed to rigorously evaluate the impact resistance of the barriers, which is crucial for determining their effectiveness in real-life situations. The detailed collection of data from these tests aimed to provide empirical evidence to support or refute the efficacy of GFRP reinforcements.

Task 3: Experiment Results Analysis
The performance of the GFRP reinforced concrete barriers was evaluated by observing the appearance of the barrier surface after direct impact and analyzing the recorded data to quantitatively analyze the deformation of the barriers. The outcomes of the observation and analysis of the GFRP reinforced barriers and the steel reinforced barriers were then compared.

2. RESEARCH PROGRAM

2.1 Specimen Construction

A total of four reinforced concrete barrier specimens were prepared and cast, including three GFRP-reinforced barriers (specimens 1, 2, and 4) and one mild steel reinforced barrier (specimen 3). To lower costs and speed up the testing process, two barriers were cast back-to-back (i.e., straight/vertical slope side facing each other) on a single concrete slab (specimens 1 and 2 on slab 1 and specimens 3 and 4 on slab 2).

2.1.1 Specimen Casting

The experimental setup involved concrete slabs measuring 6 ft. by 10 ft. with a height of eight in. These slabs serve as the base for a comprehensive barrier system and were designed to assess structural responses under controlled conditions, as shown in Figure 2.1. The barriers were attached to the slab. The slab had a thickness of 16 in. and spanned the width of the setup, forming an integral part of the structural testing framework. The slabs are reinforced with GFRP bars arranged longitudinally along the bottom of the slab at 6 in. spacing. For the first slab with specimens reinforced with GFRP bars, along the transverse direction, two rows of GFRP bar reinforcements are aligned on the top and bottom parts of the slab with a uniform interval of 6 in. Both rows of reinforcements have a concrete cover for protection purposes, with a thickness of 1.5 in. The bottom row of GFRP reinforcements extends continuously throughout the slab. In contrast, the top row is discontinued in the barrier region to accommodate the placement of stirrups, as shown in Figure 2.2(c). For the second slab, which has two barriers reinforced with GFRP and steel, the slab was reinforced with two types of reinforcements corresponding to the barriers.

The first slab had two 6ft. long barriers, with one along each side. These barriers were entirely reinforced with GFRP bars, as shown in Figure 2.2(a). The two-piece configuration was engineered to ensure a robust interconnection between the barrier and the deck. The design adhered to specific requirements: the upper part of the barrier incorporated hook-shaped bars, and the deck connection used trapezoidal stirrups. For the entire structure, a concrete cover of 1.5 in. was maintained to ensure that the reinforcement bars were adequately protected and did not protrude from the concrete. The barrier stood at a height of 34 in., while the deck measured 8 in. thick. In total, 10 straight bars ran the length of the barrier. The profile and slope of the barrier follow the Type-D MoDOT barrier design.

The second slab had the same dimensions as the first. However, one side of the deck had a barrier made with steel reinforcement while the other side was reinforced with GFRP, as shown in Figure 2.2(b). The deck reinforcement was divided into two halves, one for each material and with splicing of the two in the middle. The steel and GFRP bars along longitudinal directions were six ft long. The bars (steel & GFRP) were spliced at 12 in. The steel reinforcement follows a similar spacing to the GFRP ones. The concrete cover for all the barriers and slabs was 1.5 in. A total of 10 hook-shaped bars and 10 single trapezoidal bars were aligned along each barrier. 6 in. spacing has been held as shown in Figure 2.2. The second specimen with GFRP spiral reinforcement is the same as the first specimen reinforcement, which was manufactured by Owens Corning, and the specifications for the spiral stirrups are 10 rotations with a spacing of 6

in. between each stirrup along the 6 ft barrier length. The straight bars at the top of the spiral setup are also spaced 6 in. apart along the barrier. The other side of the slab is reinforced with steel similarly. A total of 10 spiral stirrups were fabricated using the design from our Phase I project [22]. Similarly, 10 straight bars were placed on top of the spiral stirrups, spaced evenly at 6-in. intervals along the 6-ft-long barrier.

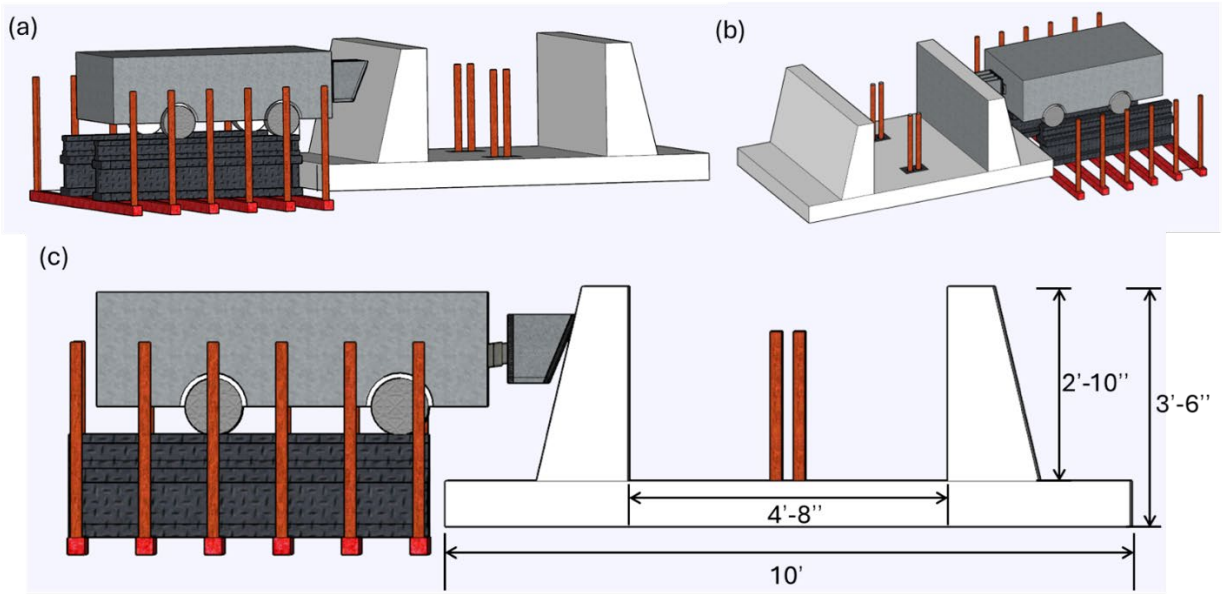

Figure 2.1 Structure overview.
(a-b) Side views of the structure of the specimens. (c) Front view.

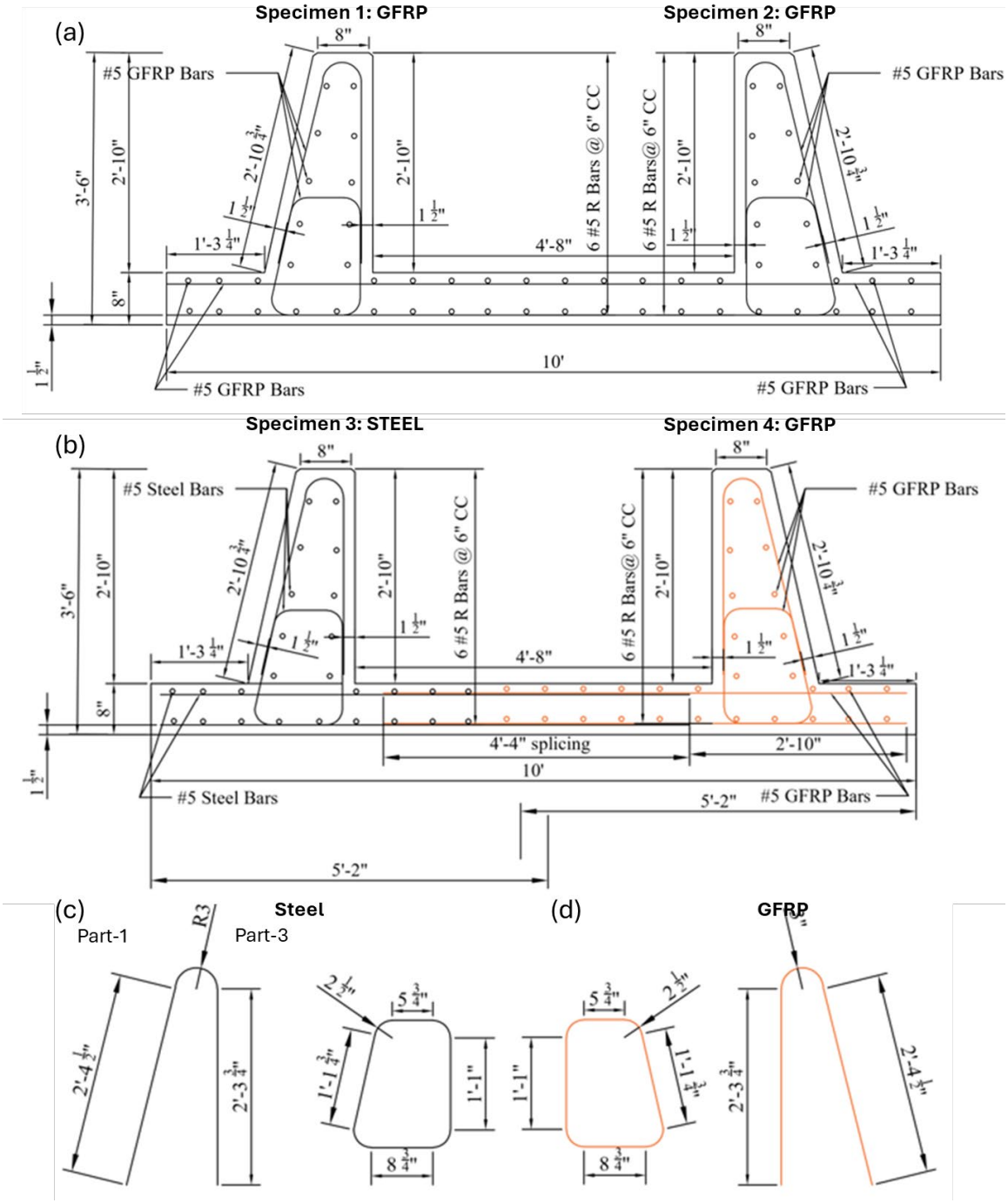

Figure 2.2 Reinforcement design.
(a-b) Specimens 1&2 and specimens 3&4. (c) Steel (specimen 3) and (d) GFRP (specimen 1,2,4) reinforcement design.

The properties of the #5 (16 mm) GFRP bar were as follows: diameter 0.625 in., nominal area 0.31 in^2, guaranteed tensile strength 116 ksi, tensile modulus 7,500 ksi, and mean ultimate strain 1.5%. The GFRP stirrup, cast into the deck and extending into the barrier, was formed as a continuous spiral tie on a mandrel. This significantly reduced manufacturing, and the team

considers that the continuous spiral tie (i.e., stirrup) would provide better confinement and load distribution across the barrier under impact load, as noted in the Phase I MoDOT study [22].

For the one steel barrier, a commercially available grade 60 ksi #5 mild steel deformed bar was used with the following properties: diameter 0.625 in., nominal area 0.3 in^2, tensile yield strength 60 ksi, tensile modulus 29,000 ksi, and yield strain 0.207%.

The concrete was formulated using two different mix ratios for the slabs (Table 2-1) and the barriers (Table 2-2). These ratios were designed in accordance with MoDOT specifications.

Table 2-1. Concrete mix ratio for slabs

	Cement	**Fly Ash**	**Sand**	**C/A**	**Water**	**Air**
Weight	580 lbf.	0	1220 lbf.	1860 lbf.	26 gallon	5.8 oz

Units: per cubic yard; C/A: coarse aggregates.

Table 2-2. Concrete mix ratio for barriers

	Cement	**Fly Ash**	**Sand**	**C/A**	**Water**	**Air**
Weight	529 lbf.	176 lbf.	1257 lbf.	1788 lbf.	30 gallon	5.8 oz

Units: per cubic yard; C/A: coarse aggregates

The 14- and 28-day compressive strengths for all four specimens were measured and recorded, as shown in Tables 2-3 through 2-6. Three groups of samples were prepared for each of the slab and barrier specimens.

Table 2-3. Compressive strength for slab 1, slab

	14 days strength (psi)	28 days strength (psi)
Sample 1	3230	4794
Sample 2	4453	5171
Sample 3	4513	4841
Average	4065	4935

Table 2-4. Compressive strength for slab 1, barriers

	14 days strength (psi)	28 days strength (psi)
Sample 1	4600	5610
Sample 2	5155	5300
Sample 3	5065	5470
Average	4940	5460

Table 2-5. Compressive strength for slab 2, slab

	14 days strength (psi)	28 days strength (psi)
Sample 1	5530	6680
Sample 2	5650	6270
Sample 3	5535	6475
Average	5570	6475

Table 2-6. Compressive strength for slab 2, barrier

	14 days strength (psi)	28 days strength (psi)
Sample 1	3115	3565
Sample 2	3165	3430
Sample 3	3010	3480
Average	3100	3490

During the casting, the slab steel reinforcement was arranged first within a steel formwork as shown in Figure 2.3. To ensure overall integrity and rigid connections between the slabs and the barrier specimens, the reinforcement for the barriers was installed before any concrete mix was poured into the formwork. Once all the reinforcement was placed, the concrete mix was poured into the formwork in the slab area and adequately vibrated to eliminate air pockets. After 28 days of curing, with the slab kept moist and at a controlled temperature, the wooden formwork for the barriers was constructed to ensure a 1.5-in. concrete cover over the barriers. After the formwork was placed, the concrete mix with the ratio indicated in Table 2-2 was poured into the formwork and allowed to cure for a 28-day period. Figures 2.3 and 2.4 show the casting processes for slab 1 with barrier specimens 1 & 2 and slab 2 with barrier specimens 3 & 4. The finished specimens are shown in Figure 2.4(d).

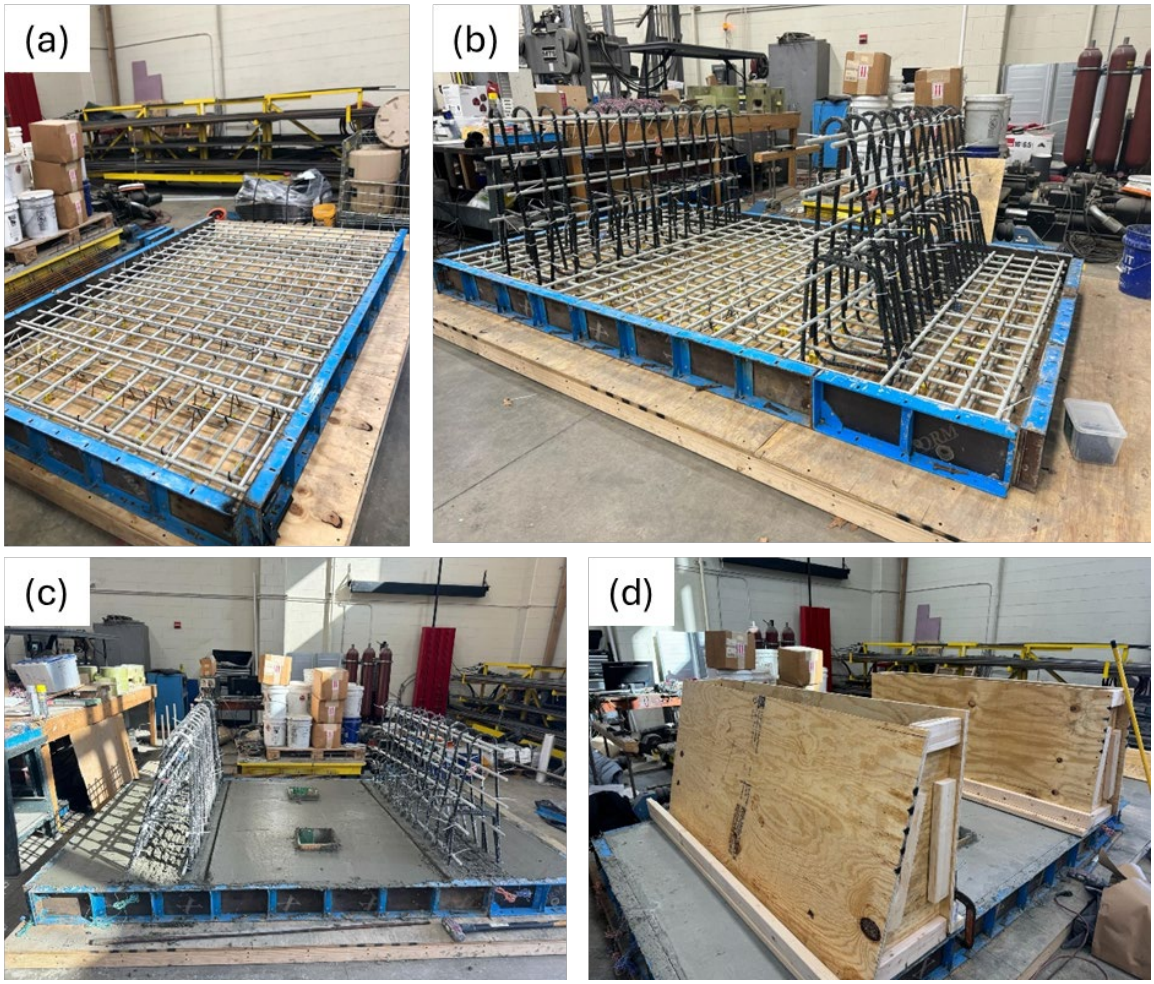

Figure 2.3 Casting procedure for slab 1 with specimens 1 & 2.

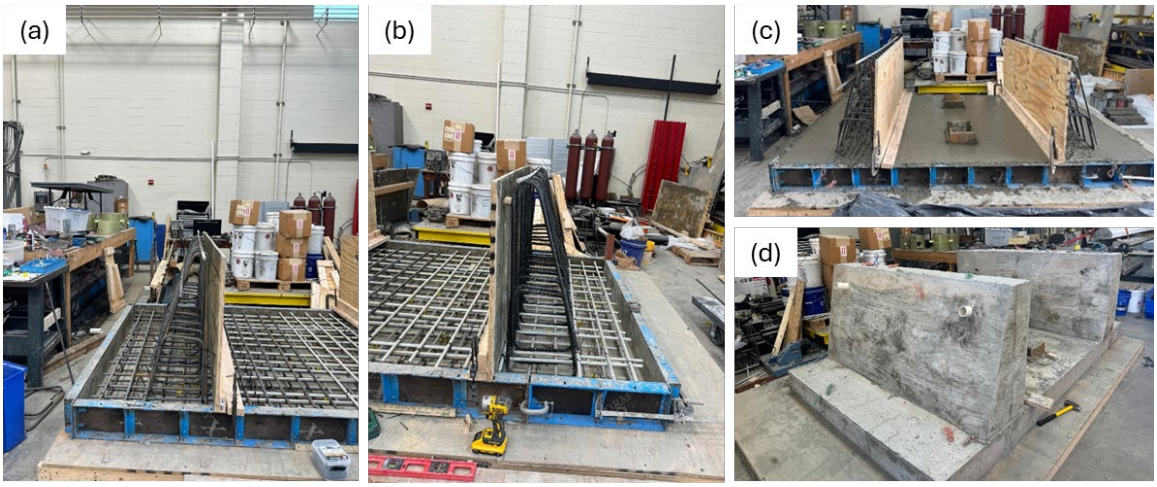

Figure 2.4 Casting procedure for slab 2 with specimens 3 & 4.

2.1.2 Impact Testing Design

The impact testing force was conducted with a cart and a specialized crash test sled system, as shown in Figure 2.5. A long, straight sled was built for testing. The height, length, and width of the sled are 7.5 ft, 20 ft, and 2 ft, respectively. The cart was weighed down with a pile of concrete blocks to increase the force of impact at the moment of the collision. The main source of momentum for the cart was gravity, while its movement was controlled by steel cables, with the self-weight of the cart being 365 lbf, and the concrete slabs used for the weighting as 296 lbf. The whole weight of the cart for the impact is 661 lbf. Considering the height of the sled system, the energy released at the impact moment, neglecting the friction-induced energy loss, is 6.7 kJ, and the velocity of the cart at impact is 21.9 ft/s.

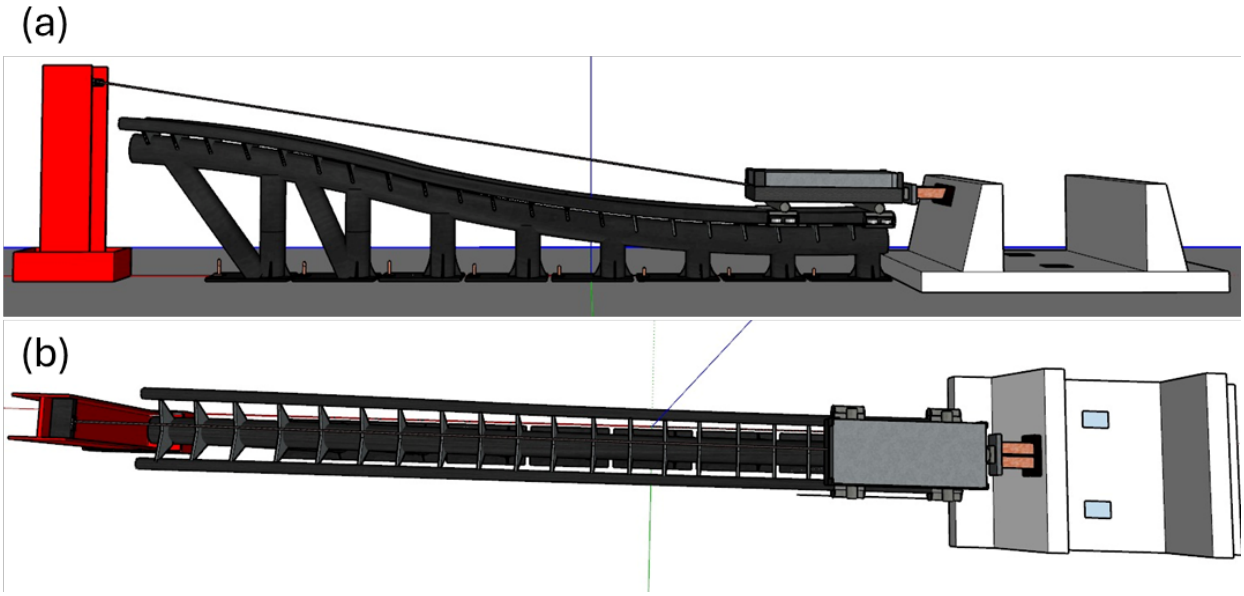

Figure 2.5 Sled system designed for the impact tests.
(a-b) Front and top view of the system.

To ensure a frontal collision between the weighted cart and the barrier, an aluminum loading wedge was installed on the barrier to withstand the impact force, as shown in Figure 2.6. The slope of the loading wedge was the same as the barrier, which was 13°.

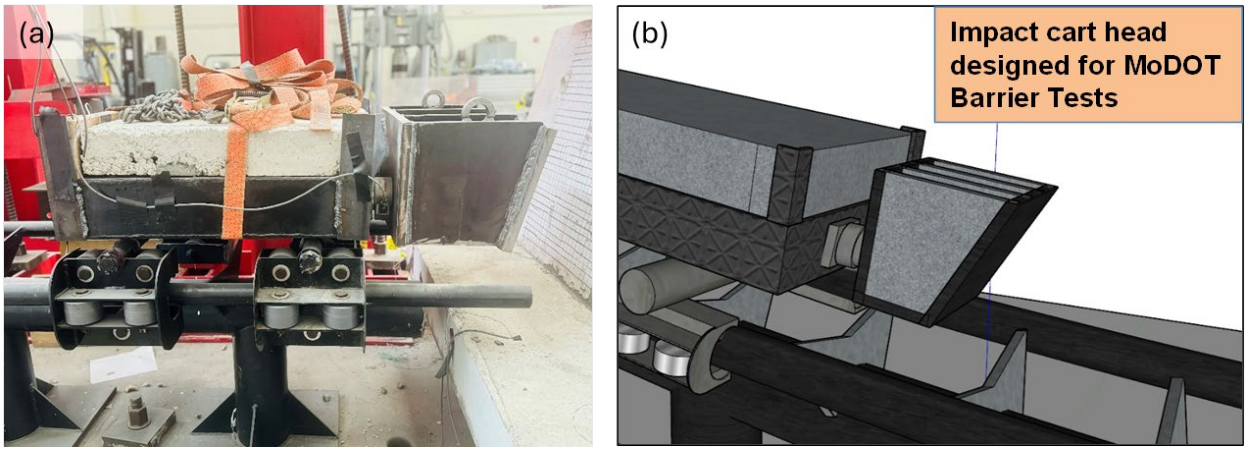

Figure 2.6 Impact test setup.
(a) Impact cart. (d) Impact cart head.

2.1.3 Measurement Approaches and Strain Gauge Design

The deformation of the barriers and forces produced from a collision needed to be recorded for quantitative analysis. In addition to the loading cell installed between the aluminum loading wedge and the barrier and imaging, a total of three systems of measurements were adopted: strain gauges, string-pots, and accelerometers.

Strain gauges were installed on the reinforcement before concrete was poured into the formwork, as shown in Figure 2.7(a). To ensure proper adhesion of the strain gauges to the reinforcement bars, the surface of the GFRP or steel reinforcements was first cleaned to remove dust, oil, or any surface contaminants. For steel reinforcements, the surface was lightly abraded using sandpaper to create a flat bonding area, while for GFRP bars, care was taken to avoid damaging the fibers during surface preparation. A suitable solvent, such as isopropyl alcohol and acetone, was then applied to clean the surface further and enhance the bonding effectiveness of the epoxy adhesive used to attach the strain gauges. After applying the epoxy and firmly placing the strain gauge, the area was covered with protective double-sided tape. This tape served to secure the gauges in position and shield them from mechanical damage during concrete casting, preventing displacement or breakage during pouring and curing. Each strain gauge was connected to lead wires using a two-wire configuration: one lead from the strain gauge was soldered to a signal wire, and the other to a return wire, ensuring accurate signal transmission.

The strain gauge instrumentation along the slab and the barriers were placed symmetrically. A total of 19 strain gauges were installed on the reinforcement throughout the barrier, providing an overall view of the inside deformation. Specifically, 10 strain gauges were installed on two barriers, and 9 were installed on slabs, with 6 placed on the longer side and 3 placed on the shorter side. The strain gauges were placed with one in the horizontal direction and one in the transverse direction.

Six strain gauges (A-SG-1 to A-SG-6) were installed on the longer edge of the slab portion, i.e., the 16-in. curb. The sizes of the curbs are 16 in. for the first specimen and 14 in. for the second specimen. These six strain gauges were aligned into two parallel rows along the longitudinal direction with distances to the edge of 12 in. Strain gauges of each row have a uniform space of 6

in. Among this group of strain gauges, A-SG-4 had two strain gauges, as did A-SG-5 and A-SG-6, with one located on the longitudinal bar and the other on the transverse bar to record strain in both directions. Three groups of strain gauges were installed on the slab at the spiral bars A-SG-1 to A-SG-3. Each group has two strain gauges close to each other and installed on longitudinal bars and transverse bars, as shown in Figure 2.7(a). The strain gauges on the barrier, which are indicated with B-SG-1 to B-SG-5, are spaced 1ft. along the barrier, leaving little space at the edges. The strain gauge's locations are at the center of the barrier along a 6 ft length. The installation is followed by the initial step of grinding the bar to create a flat surface for the epoxy to be coated, as well as for the strain gauge, to achieve a better yield. The bar is then covered with double tape.

A total of four string pots were installed on the back of the barriers to measure the deformation of the barriers from the outside. The string pots were all positioned along the centerline of the barriers and distributed vertically along their height, as shown in Figure 2.7(b). String Pots 1 and 4 were installed on top and bottom of the back of the barrier, while String Pots 2 and 3 were installed at 1/3 and 1/2 of the back, counting from the top. The installation of the string pots was carried out in multiple stages. First, a frame made of plywood was assembled and positioned at the center of the specimen. String pots were then mounted at specific heights—top, one-third, half, and bottom of the barrier—to capture a linear response pattern after impact. On the opposite side, the back face of the barrier, a steel plate was bonded to the concrete using epoxy to ensure firm adhesion and improve the accuracy of impact results.

A total of three accelerometers were installed on the back of the barriers to measure the strain rate change under the impact. The accelerometers were distributed along the horizontal direction of the barrier, as shown in Figure 2.7(c). The accelerometers 1, 2, 3 were placed 18, 36, and 54 in. from the left edge.

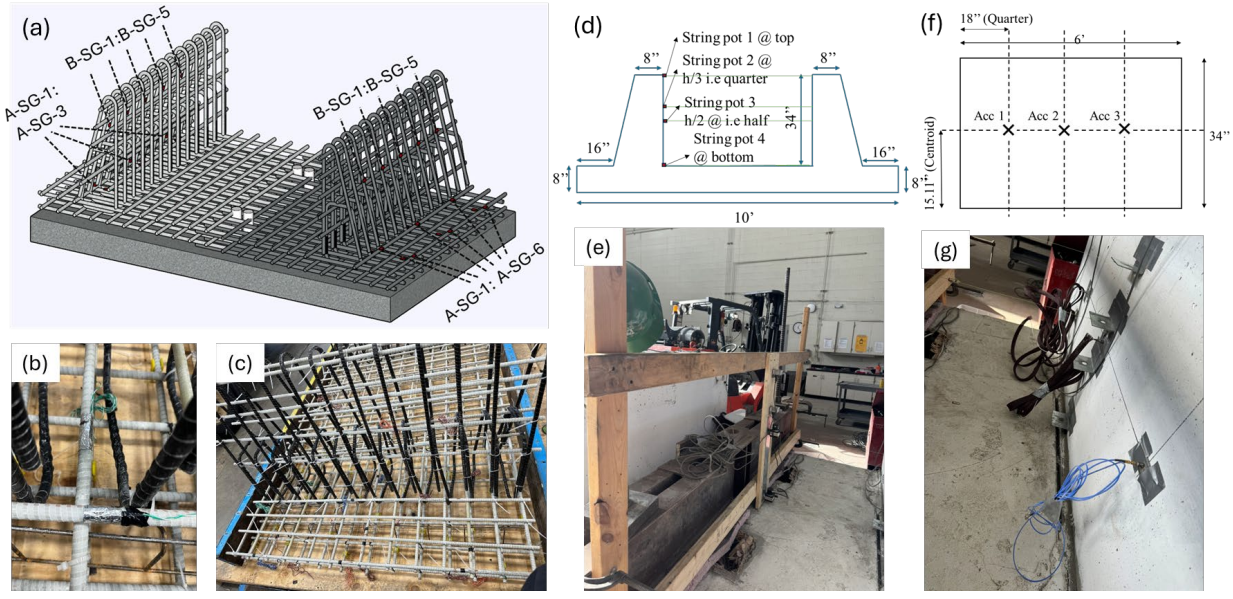

Figure 2.7 Impact test measurement setups.
(a-c) Locations and installations of strain gauges. (d-e) Locations and installations of string pots. (f-g) Locations and installations of accelerometers.

2.2 Impact Test

The impact tests were conducted to investigate the dynamic performance of the concrete barriers reinforced with different materials in a high bay laboratory on several separate days ranging from January 13th to 22nd, 2025. The sled system used for the impact testing has a length of 20 ft, a width of 2 ft, and a height of 7.5 ft. The impact zone area on the surface of the barrier was indicated with a grid or frame that has dimensions of 12 in. x 24 in., which is also the size of the impact plate. The cart used for the impact had a total weight of 661 lbs. High-speed cameras were used to capture the whole process, especially the impact moment. For each of the four barriers, a total of three loading conditions were considered: tap, where the cart was initially placed very close to the barrier and the impact was conducted under a low speed to test whether the whole system could work as expected; one-third case, where the cart was initially lifted to one third of the overall height of the sled system and then released to impact the barrier; two-thirds case where the cart was initially lifted to two thirds of the sled.

The status of the three GFRP-reinforced and the one steel-reinforced barriers after the impact testing is shown in Figures 2.8-2.11. In all cases other than specimen 2, no apparent damage or visible cracks were observed at or around the impact area, but only scratches were observed in the direct impact area. The partially concrete missing after the impact in specimen 2 is caused by the relatively low bonding strength between the concrete cover and the reinforcement, rather than an overall structural failure. This validates the capability of the barriers to withstand the impact force while also maintaining serviceability.

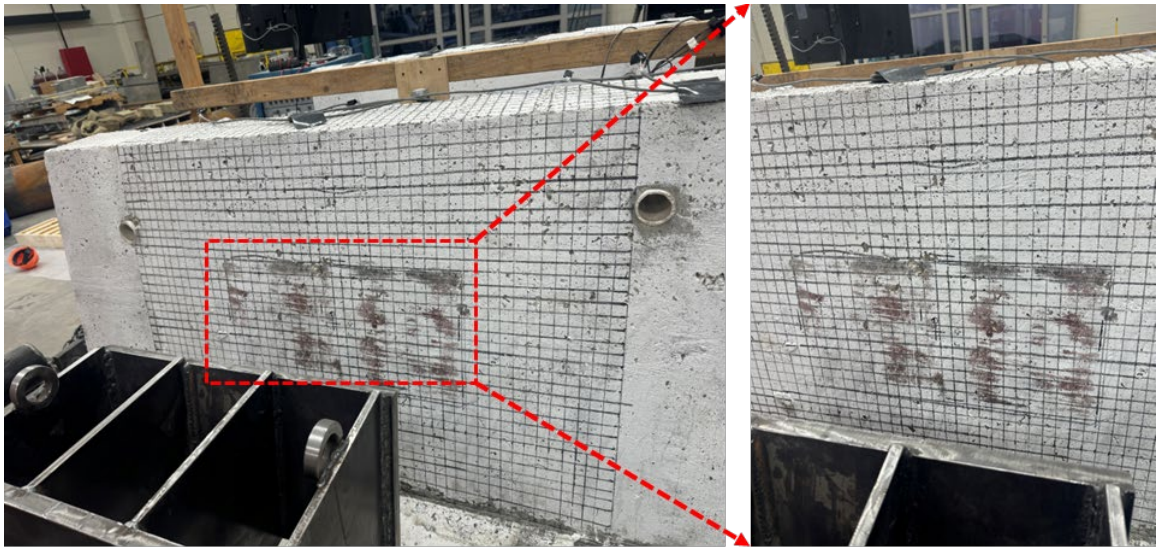

Figure 2.8 Barrier of specimen 1 (GFRP) after the impact testing.

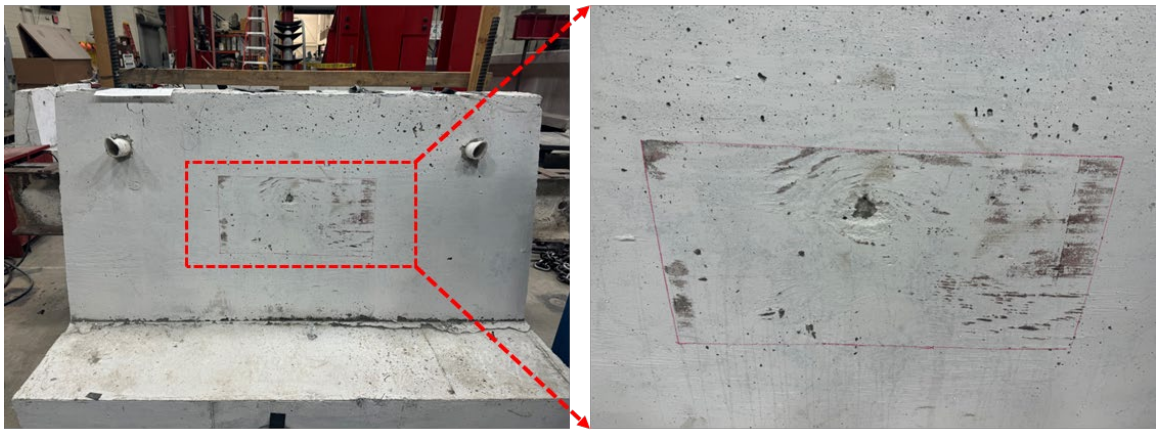

Figure 2.9 Barrier of specimen 2 (GFRP) after the impact testing.

Figure 2.10 Barrier of specimen 3 (Steel) after the impact testing.

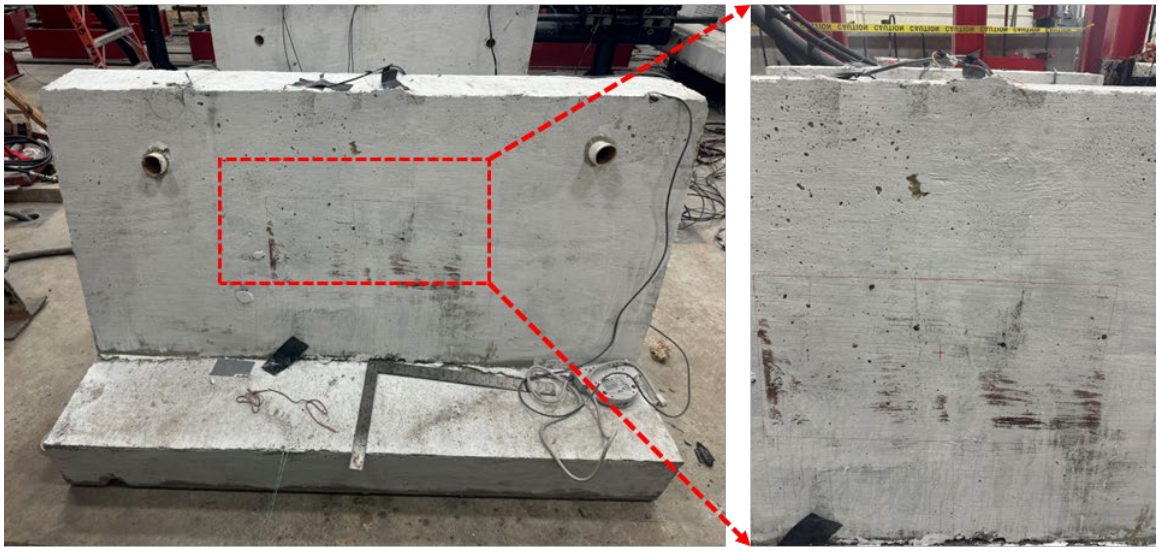

Figure 2.11 Barrier of specimen 4 (GFRP) after the impact testing.

2.3 Results and Analysis

For quantitative analysis purposes, the load, displacement, and strain changes during the impact testing process were recorded or measured using the load cell, string pots, and strain gauges. Load changes of all four barrier specimens (1,2,4 reinforced with GFRP and 3 reinforced with steel) of two-thirds cases were recorded with loading cells and shown in Figure 2.12. Each curve exhibits a sharp peak indicating the maximum force caused by the impact of the cart. The GFRP samples show varying peak forces, with GFRP-2 having a peak force that is significantly higher than that of GFRP-1 and 3. The steel sample's peak force is markedly lower than the highest value of the GFRP samples (GFRP-2) but larger than the others (GFRP-1 and 2), indicating a similar impact force for all cases with different reinforcement. After reaching their peaks, all curves rapidly decline to lower force levels, with minor fluctuations. All significant changes of the force for all cases occurred within the first two seconds after the peak values.

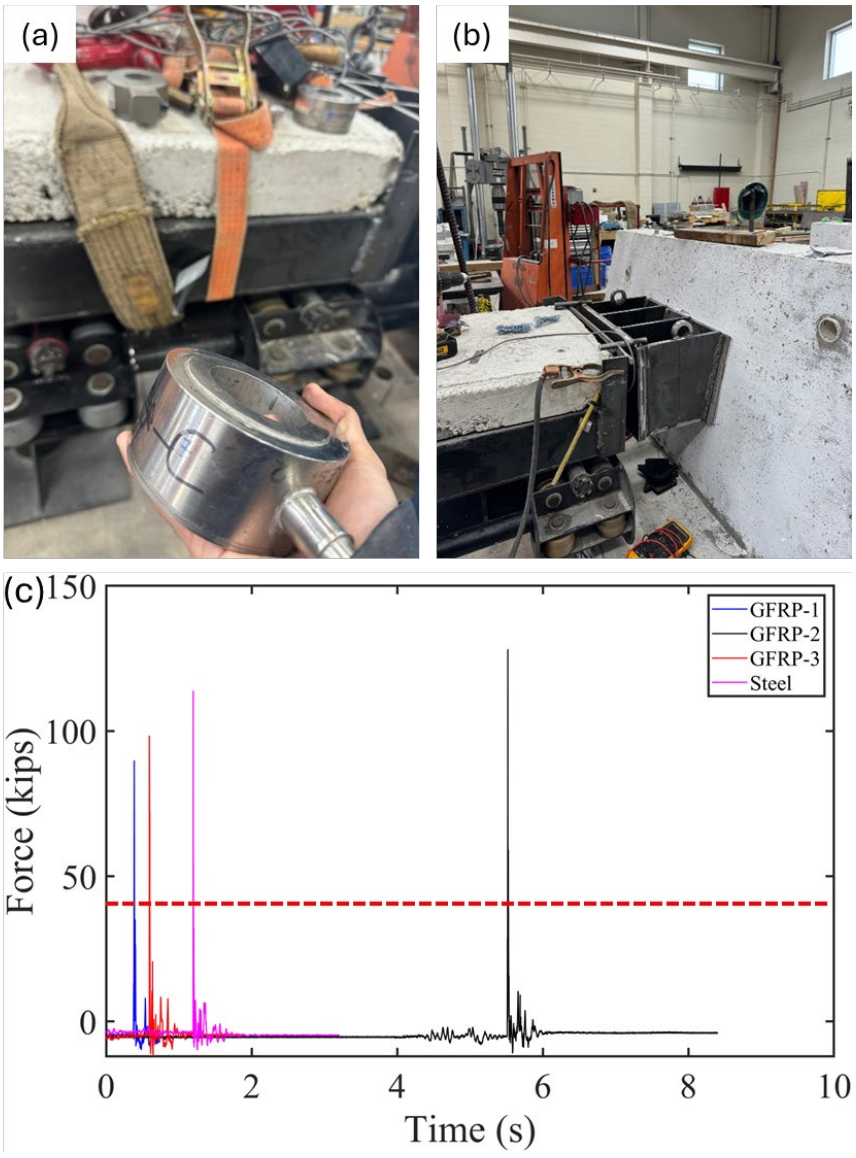

Figure 2.12 Force measurements.
(a-b). Loading cell installed on the barrier. (c) Measured forces in the impact testing. The red line indicates the static design load.

The installed accelerometers are shown in Figure 2.13(a) while the measured accelerations are shown in Figure 2.13(c). Initially, there is a sharp spike in acceleration for all materials. GFRP-2 displays the most significant initial peaks, indicating a rapid acceleration. It then swiftly declines to stabilization. This corresponds to the maximum peak force observed for GFRP-2 in Figure 2.12. Meanwhile, GFRP-1 and 3 have much smaller initial peaks followed by a similar rapid decrease. Acceleration for the steel sample shows a more moderate and stable response with the most moderate amplitude among the samples tested. Following these initial peaks, all curves quickly return toward zero, suggesting that the materials stop accelerating almost immediately after the impact, indicating a stable structure that is resistant to the impact for all cases.

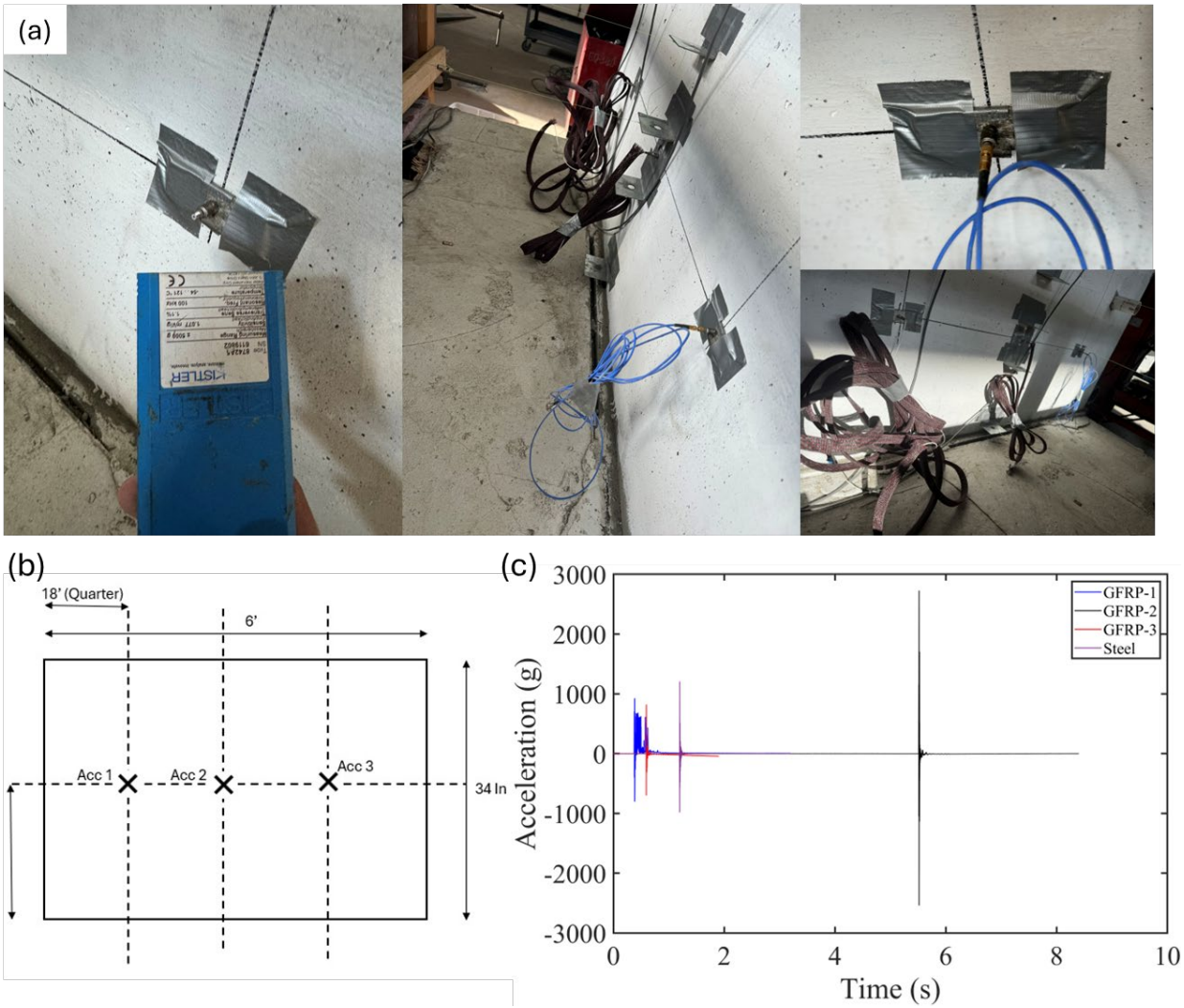

Figure 2.13 Acceleration measurements.
(a). Installed accelerometer. (b) Locations of accelerometers. (c) Measured accelerations.

Figure 2.14 shows the displacement changes measured from the four string pots for all specimens. For all measurement locations and test cases, the displacement responses consistently exhibited peak values corresponding to the moment of impact. Among them, the GFRP-2 case recorded the largest initial displacement, indicating the highest structural response. In contrast, the GFRP-1 and GFRP-3 cases showed significantly smaller displacement changes. The steel-

reinforced case exhibited a moderate peak displacement, suggesting an intermediate level of flexibility and energy absorption. The peak displacement values for all cases are at the same level, showing a similar impact resistance for all cases with different types of reinforcement materials. The steel sample in all graphs shows the least variation in displacement change, indicating its slightly higher stiffness to deformation under similar loading conditions compared to the GFRP samples. The maximum displacement peak of all cases is no larger than 0.2 in. and then rapidly decreases to a value close to 0, indicating the excellent properties of impact resistance and quick recovery. This is consistent with the fact that no obvious damage or cracks were observed at or around the direct impact areas after the testing for all cases. The displacement value lower than 0.05 in. after stabilization for all four string pot measurements of the steel reinforcement case is caused by an overall displacement of a loosened anchor rather than the deformation of the barrier.

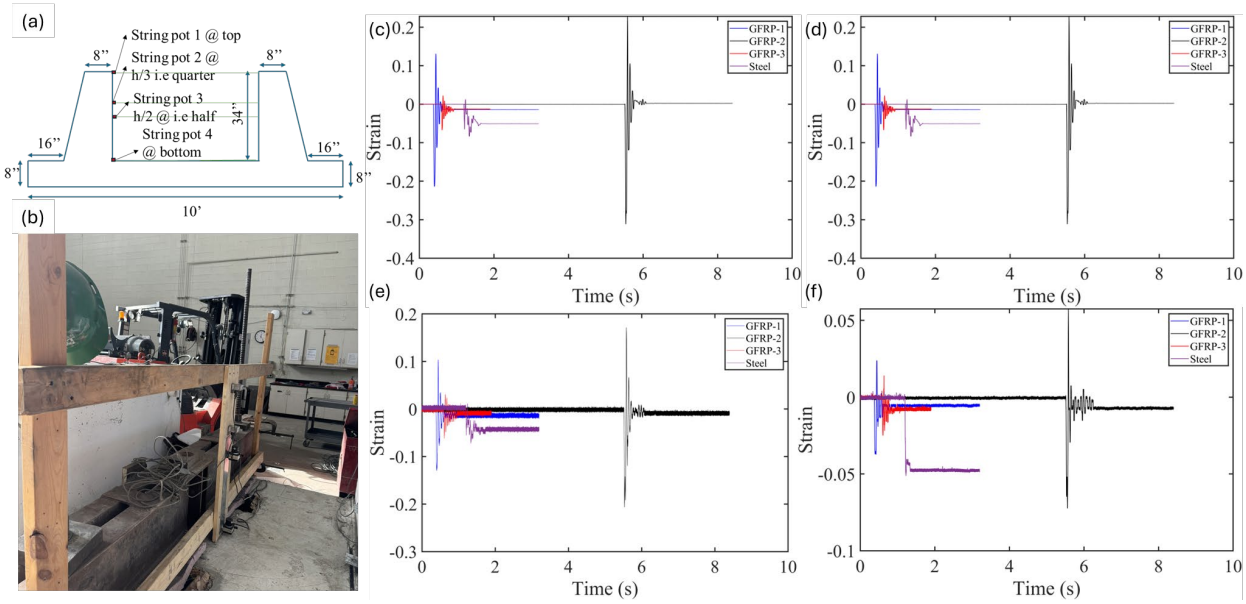

Figure 2.14 Displacement measurements on the back of the barriers. (a) Locations and (b) installed string pots. (c-f) Measured displacements at locations of String Pots 1-4.

To track the deformation inside the barrier during the impact testing, strain gauges were installed on the surfaces of the reinforcement before the concrete was poured into the formwork. The strain gauges were distributed throughout the reinforcement of the barrier. Before the final test, 10 out of 17 strain gauges were able to function and output strain data. The recorded strain changes over time for specimen 1 (GFRP) are shown in Figure 2.15. It shows that the largest strain is recorded by gauge 10, which is located within the direct impact area. All recorded strain values are below 2.0e-3, which is less than the compressive strain limit of steel reinforcement.

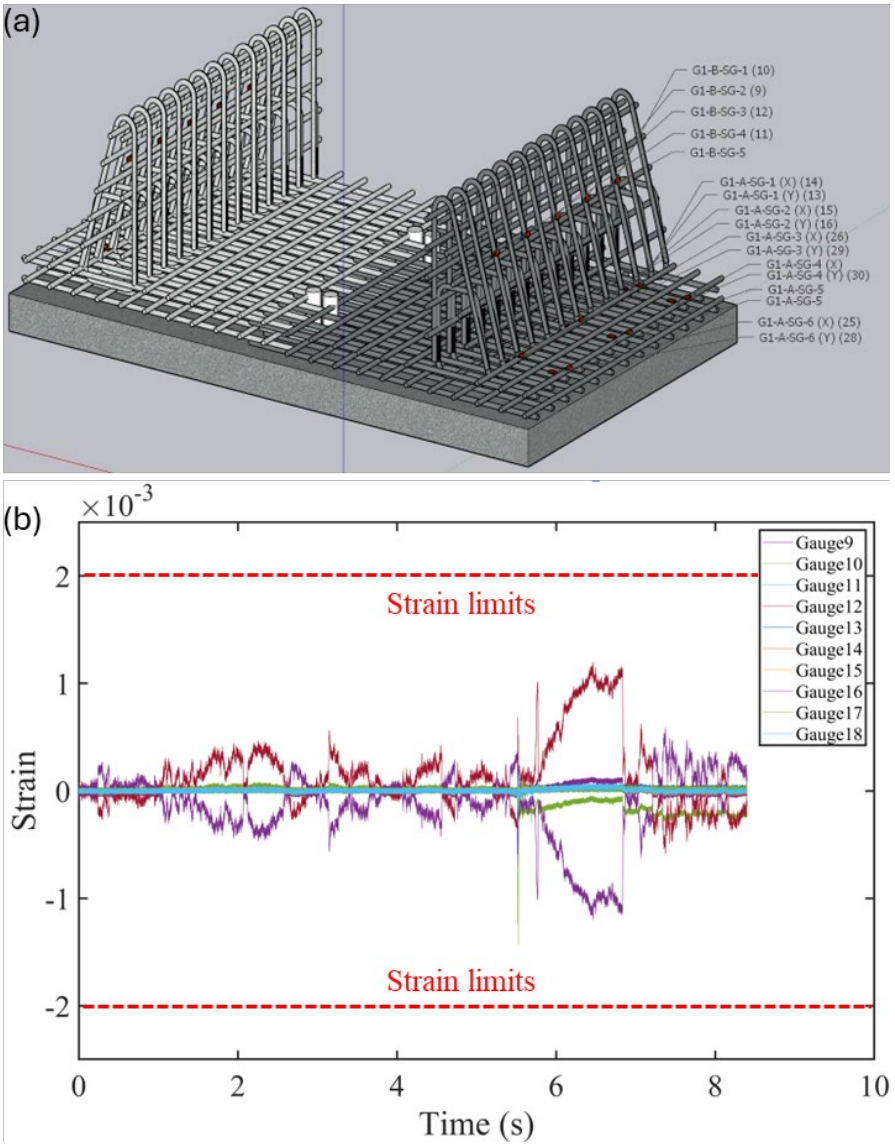

Figure 2.15 Strain measurements inside barrier specimen 1.
(a) Strain gauges deployed on the GFRP reinforcements. (b) Measured strains.

3. CONCLUSIONS AND RECOMMENDATIONS

This study on GFRP-reinforced concrete barriers successfully prepared a total of four reinforced concrete barriers, including three specimens reinforced with GFRP and one reinforced with steel for comparison consideration. The impact testing was conducted by utilizing a cart with weights on a straight, long sled system. The strain gauge, string pot, accelerometer systems, and loading cells were utilized to evaluate the performance of the GFRP-reinforced barrier specimens quantitatively and to compare that performance to the traditional steel reinforced barriers.

The results showed that GFRP reinforced barrier specimens are fully capable of withstanding the potential impact loading conditions that could happen in real-world applications. With the cart impact force above the minimum MASH peak impact load required for the test, no obvious cracks or damage were observed within the direct impact domain for any of these four specimens; the structure remained intact after the testing. The strains recorded were below the warning limit, and the peaks caused by the impact reduced to around zero in a very short period of time.

Future recommendations include a Phase III research deployment where MoDOT implements a steel-free bridge deck and barrier system validated in this Phase II MoDOT study. The scope of the deployment could be limited to single or multiple bridge-type systems, including reinforced concrete slab bridges, reinforced concrete beam bridges, prestressed concrete girder bridges, and steel girder bridges with reinforced concrete bridge decks. For a Phase III deployment project(s), the key recommended research tasks to be included by the research teams are as follows:

- Provide technical expertise in the design of the bridge, including the bridge barrier, bridge deck, and integration of the barrier, deck, and girder interface shear transfer between the components using GFRP.
- Finite element method (FEM) modeling of the bridge(s) to supplement traditional design assumptions and provide design verification/redundancy.
- Assist the contractor in the construction and fabrication of the bridge(s), including the coordination of instrumentation and sensors for load testing and monitoring of the bridge(s).
- Following the construction of the bridge(s), implement a load testing program to study the load distribution of bridge deck loading due to the variation in the deck and barrier GFRP reinforcement stiffness. This will develop recommendations for load distribution, like the current American Association of State Highway and Transportation Officials (AASHTO) recommendations for mild steel reinforced bridge decks. Further examine the serviceability of the structure(s) compared to FEM and design calculations. A FEM parametric investigation will be conducted to further support this physical load testing.
- Over a set period of in-service performance (one- to two-year minimum is recommended) investigate the thermal behavior of these bridge systems to document the thermal changes and behavior of these structures. Recommendations for any variations in thermal stresses may be developed and provided.
- Over a set period of in-service performance (one- to two-year minimum is recommended) investigate the variation in strain and stress in the bridge(s) due to service level loads and any recommended future design considerations.

- Investigate the interest to develop this proposed Phase III study as a pool fund study with multiple DOTs to expand the deployment of GFRP barrier systems with possible states such as Missouri, Florida, Texas, California, and Ohio to name a few that have worked to develop their own barrier systems and are also awaiting wider implementation.

Consider a future Phase IV study to examine repair/retrofit techniques should damage occur to GFRP barriers due to overweight vehicle impact outside of the TL level design for these barriers.

4. REFERENCES

1. Zain, M.F.B.M. and H.J. Mohammed, *Concrete road barriers subjected to impact loads: An overview.* Latin American Journal of Solids and Structures, 2015. **12**: p. 1824-1858.
2. Elchalakani, M., T. Aly, and E. Abu-Aisheh, *Mechanical properties of rubberised concrete for road side barriers.* Australian Journal of Civil Engineering, 2016. **14**(1): p. 1-12.
3. Shen, W., et al., *Investigation on the safety concrete for highway crash barrier.* Construction and building materials, 2014. **70**: p. 394-398.
4. Lokken, E.C., *Concrete safety barrier design.* Transportation Engineering Journal of ASCE, 1974. **100**(1): p. 151-168.
5. Albuquerque, F.D.B. and D.L. Sicking, *In-service safety performance evaluation of roadside concrete barriers.* Journal of transportation safety & security, 2013. **5**(2): p. 148-164.
6. Böhni, H., *Corrosion in reinforced concrete structures*. 2005: Woodhead publishing.
7. Song, H.-W. and V. Saraswathy, *Corrosion monitoring of reinforced concrete structures–a review.* International journal of electrochemical science, 2007. **2**(1): p. 1-28.
8. Rodrigues, R., et al., *Reinforced concrete structures: A review of corrosion mechanisms and advances in electrical methods for corrosion monitoring.* Construction and Building Materials, 2021. **269**: p. 121240.
9. Wei, C., C.S. Wojnar, and C. Wu, *Hydro-chemo-mechanical phase field formulation for corrosion induced cracking in reinforced concrete.* Cement and Concrete Research, 2021. **144**: p. 106404.
10. Capozucca, R., *Damage to reinforced concrete due to reinforcement corrosion.* Construction and Building Materials, 1995. **9**(5): p. 295-303.
11. Nkurunziza, G., et al., *Durability of GFRP bars: A critical review of the literature.* Progress in structural engineering and materials, 2005. **7**(4): p. 194-209.
12. Alabtah, F.G., E. Mahdi, and M. Khraisheh, *External corrosion behavior of steel/gfrp composite pipes in harsh conditions.* Materials, 2021. **14**(21): p. 6501.
13. Fujii, Y., et al. *Durability of GFRP in corrosive environment*. in *ISOPE International Ocean and Polar Engineering Conference*. 1993. ISOPE.
14. Mufti, A., et al. *Durability of GFRP reinforced concrete in field structures*. in *Proc., 7th Int. Symp. on Fiber-Reinforced Polymer (FRP) Reinforcement for Concrete Structures (FRPRCS)*. 2005. American Concrete Institute Farmington Hills, MI.
15. Yan, F., Z. Lin, and M. Yang, *Bond mechanism and bond strength of GFRP bars to concrete: A review.* Composites Part B: Engineering, 2016. **98**: p. 56-69.
16. Benmokrane, B., O. Chaallal, and R. Masmoudi, *Glass fibre reinforced plastic (GFRP) rebars for concrete structures.* Construction and Building Materials, 1995. **9**(6): p. 353-364.
17. Toutanji, H.A. and M. Saafi, *Flexural behavior of concrete beams reinforced with glass fiber-reinforced polymer (GFRP) bars.* Structural Journal, 2000. **97**(5): p. 712-719.
18. Neves, R.R., et al., *Performance of some basic types of road barriers subjected to the collision of a light vehicle.* Journal of the Brazilian Society of Mechanical Sciences and Engineering, 2018. **40**(6): p. 274.
19. MacDonald, D.J. and A.R. Kirk, *Precast concrete barrier crash testing*. 2001, Oregon. Dept. of Transportation. Research Group.
20. Consolazio, G.R., J.H. Chung, and K.R. Gurley, *Impact simulation and full scale crash testing of a low profile concrete work zone barrier.* Computers & structures, 2003. **81**(13): p. 1359-1374.

21. Transportation, C.D.o., *CRASH TESTING OF VARIOUS TEXTURED BARRIERS* 2002.
22. Wei, C., J. Myers, and C. Wu, *GFRP Reinforced Bridge Barriers: Numerical Modeling*. 2022, Missouri. Department of Transportation. Construction and Materials Division.